Entanglement and superposition states in the micromaser

H. Walther

Email alerting service	Receive free email alerts when new articles cite this article - sign up in the box at the top right-hand corner of the article or click **here**

Entanglement and superposition states in the micromaser

By H. Walther

Sektion Physik der Universität München and Max–Planck-Institut für
Quantenoptik, 85748 Garching, Germany

In this paper recent experiments with the one-atom maser or micromaser are
reviewed. They deal with the dynamical behaviour of the field at parameter val-
ues where the field undergoes phase transitions. Furthermore, atomic interferences
are observed in the micromaser when the inversion of the atoms leaving the cavity
is measured while the cavity frequency is scanned across the atomic resonance. The
interferences are due to the non-adiabatic mixing of dressed states at the entrance
and exit holes of the maser cavity. The interference structures are triangular shaped
and approximately equidistant. They are associated with the dynamics of the atom–
field interaction, show quantum jumps and demonstrate bistability of the micromaser
field.

1. Introduction

The one-atom maser or micromaser is an ideal instrument for the study of the reso-
nant interaction of a single atom with a single mode of a superconducting niobium
cavity (Meschede et $al.$ 1985; Rempe et $al.$ 1987, 1990; Rempe & Walther 1990). In
the experiments values of the quality factor as high as 3×10^{10} have been achieved
for the resonant mode, corresponding to an average lifetime of a photon in the cav-
ity of 0.2 s. The photon lifetime is thus much longer than the interaction time of
an atom with the maser field; during the atom passes through the cavity the only
change of the cavity field that occurs is due to the atom–field interaction. The atoms
used in the experiments are rubidium Rydberg atoms pumped by laser excitation
into the upper level of the maser transition, which is usually induced between neigh-
bouring Rydberg states. In the experiments, the atom–field interaction is probed
by observing the population in the upper and lower maser levels after the atoms
have left the cavity. The field in the cavity consists only of single or a few photons
depending on the atomic flux. Nevertheless, it is possible to study the interaction
in considerable detail. The dynamics of the atom–field interaction treated with the
Jaynes–Cummings model was investigated by selecting and varying the velocity of
the pump atoms (Rempe et $al.$ 1987). The counting statistics of the pump atoms
emerging from the cavity allowed us to measure the non-classical character of the
cavity field (Rempe et $al.$ 1990; Rempe & Walther 1990) predicted by the micromaser
theory. The maser field can be investigated in this way since there is entanglement
between the maser field and the state in which the atom leaves the cavity (Wagner
et $al.$ 1993; Löffler et $al.$ 1996). It also has been observed that under suitable exper-
imental conditions the maser field exhibits metastability and hysteresis (Benson et

al. 1994). Most of the maser experiments so far have been performed at cavity temperatures of 0.5 K. Recently, a further reduction of the temperature to below 0.1 K was achieved by using an improved set-up in a dilution refrigerator (Benson *et al.* 1994).

In the following we are going to review two recent experiments which deal with the observation of quantum jumps of the micromaser field and with the observation of atomic interferences in the cavity (Raithel *et al.* 1995). New experiments on the correlation of atoms after the interaction with the cavity field will be briefly mentioned. For a review of the previous work see Raithel *et al.* (1994).

2. Quantum jumps and atomic interferences in the micromaser

Under steady-state conditions, the photon statistics $P(n)$ of the field is essentially determined by the pump parameter, $\Theta = \frac{1}{2}N_{\mathrm{ex}}^{1/2}\Omega t_{\mathrm{int}}$ (Filipowicz *et al.* 1986; Lugiato *et al.* 1987; Raithel *et al.* 1994). Here, N_{ex} is the average number of atoms that enter the cavity during τ_{cav}, Ω the vacuum Rabi flopping frequency, and t_{int} is the atom–cavity interaction time. The quantity $\langle\nu\rangle = \langle n\rangle/N_{\mathrm{ex}}$ shows the following generic behaviour (see figure 1): it suddenly increases at the maser threshold value $\Theta = 1$, and reaches a maximum for $\Theta \approx 2$ (denoted by A in figure 1). The maser threshold shows the characteristics of a continuous phase transition (Filipowicz *et al.* 1986; Lugiato *et al.* 1987). As Θ further increases, $\langle\nu\rangle$ decreases and reaches a minimum at $\Theta \approx 2\pi$, and then abruptly increases to a second maximum (B in figure 1). This general type of behaviour recurs roughly at integer multiples of 2π, but becomes less pronounced with increasing Θ. The reason for the periodic maxima of $\langle\nu\rangle$ is that for integer multiples of $\Theta = 2\pi$, the pump atoms perform an almost integer number of full Rabi flopping cycles, and start to flip over at a slightly larger value of Θ, thus leading to enhanced photon emission. The periodic maxima in $\langle\nu\rangle$ for $\Theta = 2\pi$, 4π, ..., can be interpreted as first-order phase transitions (Filipowicz *et al.* 1986; Lugiato *et al.* 1987). The field strongly fluctuates for all phase transitions (A, B and C in figure 1), the large photon number fluctuations for $\Theta \approx 2\pi$ and multiples thereof being caused by the presence of two maxima in the photon number distribution $P(n)$ at photon numbers n_{l} and n_{h} ($n_{\mathrm{l}} < n_{\mathrm{h}}$). For n_{l} and n_{h}, the atoms perform almost integer numbers m or $m + 1$ of full Rabi flopping cycles, respectively. If the pump parameter is scanned across $\Theta \approx 2\pi m$, the maximum of $P(n)$ at n_{l} completely dies out, and is replaced by the new peak at the higher photon number n_{h}. For $\Theta \approx 2\pi m$, the simultaneous presence of two maxima of $P(n)$ leads to spontaneous jumps of the micromaser field between two average photon numbers n_{l} and n_{h}.

The phenomenon of the two coexisting maxima in $P(n)$ was also studied in a semiheuristic Fokker–Planck (FP) approach (Filipowicz *et al.* 1986; Lugiato *et al.* 1987). There, the photon number distribution $P(n)$ is replaced by a probability function $P(\nu, \tau)$ with continuous variables $\tau = t/\tau_{\mathrm{cav}}$ and $\nu(n) = n/N_{\mathrm{ex}}$, the latter replacing the photon number n. The steady-state solution obtained for $P(\nu, \tau)$, $\tau \gg 1$, can be constructed by means of an effective potential $V(\nu)$ showing minima at positions where maxima of $P(\nu, \tau)$, $\tau \gg 1$, are found. Close to $\Theta = 2\pi$ and multiples thereof, the effective potential $V(\nu)$ exhibits two equally attractive minima located at stable gain–loss equilibrium points of maser operation (Meystre 1992) (see figure 1). The mechanism at the phase transitions mentioned is always the same: a minimum of $V(\nu)$ loses its global character when Θ is increased, and is replaced in this role by the next one. This reasoning is a variation of the Landau theory of first-order phase
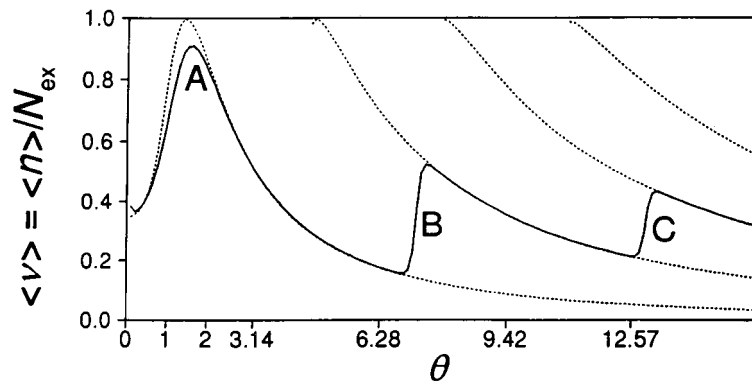
Figure 1. Mean value of $\nu = n/N_{\mathrm{ex}}$ versus the pump parameter $\Theta = \Omega t_{\mathrm{int}}\sqrt{N_{\mathrm{ex}}}/2$, where the value of Θ is changed via N_{ex}. The solid line represents the micromaser solution for $\Omega = 36$ kHz, $t_{\mathrm{int}} = 35\,\mu$s and temperature $T = 0.15$ K. The dotted lines are semiclassical steady-state solutions corresponding to fixed stable gain = loss equilibrium photon numbers (Meystre 1992). The crossing points between a line $\Theta =$ const. and the dotted lines correspond to the values where minima in the Fokker–Planck potential $V(\nu)$ occur.

transitions, with $\sqrt{\nu}$ being the order parameter. This analogy actually leads to the notion that in the limit $N_{\mathrm{ex}} \to \infty$ the change of the micromaser field around integer multiples $\Theta = 2\pi$ can be interpreted as first-order phase transitions.

Close to first-order phase transitions, long field evolution time constants τ_{field} are expected (Filipowicz *et al.* 1986; Lugiato *et al.* 1987). This phenomenon is experimentally demonstrated in this paper, as well as related phenomena, such as spontaneous quantum jumps between equally attractive minima of $V(\nu)$, bistability and hysteresis. Some of those phenomena are also predicted in the two-photon micromaser (Raithel *et al.* 1995), for which qualitative evidence of first-order phase transitions and hysteresis is reported (Raimond *et al.* 1989).

The experimental set-up used is shown in figure 2. It is similar to that described by Rempe & Walther (1990) and Benson *et al.* (1994). As before, ^{85}Rb atoms were used to pump the maser. They are excited from the $5S_{1/2}$, $F = 3$ ground state to $63P_{3/2}$, $m_{\mathrm{J}} = \pm\frac{1}{2}$ states by linearly polarized light of a frequency-doubled c.w. ring dye laser. The polarization of the laser light is linear and parallel to the likewise linearly polarized maser field, and therefore only $\Delta m_{\mathrm{J}} = 0$ transitions are excited. Superconducting niobium cavities resonant with the transition to the $61D_{3/2}$, $m_{\mathrm{J}} = \pm\frac{1}{2}$ states were used; the corresponding resonance frequency is 21.506 GHz. The experiments were performed in a ^{3}He/^{4}He dilution refrigerator with cavity temperatures $T \approx 0.15$ K. The cavity Q values ranged from 4×10^9 to 8×10^9. The velocity of the Rydberg atoms and thus their interaction time t_{int} with the cavity field were preselected by exciting a particular velocity subgroup with the laser. For this purpose, the laser beam irradiated the atomic beam at an angle of approximately $82°$. As a consequence, the UV laser light (linewidth *ca.* 2 MHz) is blue-shifted by 50–200 MHz by the Doppler effect, depending on the velocity of the atoms.

Information on the maser field and interaction of the atoms in the cavity can be obtained solely by state-selective field ionization of the atoms in the upper or lower maser level after they have passed through the cavity. The field ionization detector was recently modified, so that there is now a detection efficiency of $\eta = (35\pm5)\%$. For different t_{int}, the atomic inversion has been measured as a function of the pump rate
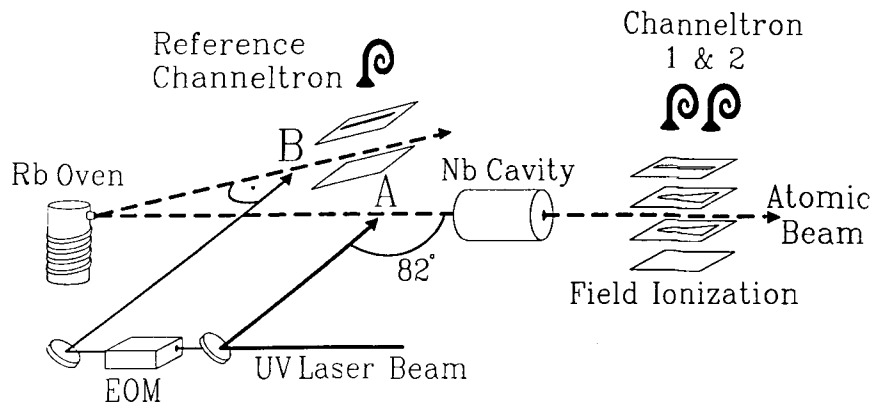
Figure 2. Sketch of the experimental set-up. The rubidium atoms emerge from an atomic beam oven and are excited at an angle of 82° at location A. After interaction with the cavity field, they enter a state-selective field ionization region, where channeltrons 1 and 2 detect atoms in the upper and lower maser levels, respectively. A small fraction of the UV radiation passes through an electro-optic modulator (EOM), which generates sidebands of the UV radiation. The blue-shifted sideband is used to stabilize the frequency of the laser onto the Doppler-free resonance monitored with a secondary atomic beam produced by the same oven (location B).

by comparing the results with micromaser theory (Filipowicz *et al.* 1986; Lugiato *et al.* 1987), the coupling constant Ω is found to be $\Omega = (40 \pm 10)$ krad s^{-1}.

Depending on the parameter range, essentially three regimes of the field evolution time constant τ_{field} can be distinguished. Here we only discuss the results for intermediate time constants. The maser was operated under steady-state conditions close to the second first-order phase transition (C in figure 1). The interaction time was $t_{\text{int}} = 47\,\mu\text{s}$ and the cavity decay time $\tau_{\text{cav}} = 60$ ms. The value of N_{ex} necessary to reach the second first-order phase transition was $N_{\text{ex}} \approx 200$. For these parameters, the two maxima in $P(n)$ are manifested in spontaneous jumps of the maser field between the two maxima with a time constant of *ca.* 5 s. This fact and the relatively large pump rate led to the clearly observable field jumps shown in figure 3. Because of the large cavity field decay time, the average number of atoms in the cavity was still as low as 0.17. The two discrete values for the counting rates correspond to the metastable operating points of the maser, which correspond to *ca.* 70 and *ca.* 140 photons. In the FP description, the two values correspond to two equally attractive minima in the FP potential $V(\nu)$. If one considers, for instance, the counting rate of lower-state atoms (CT2 in figure 3), the lower (higher) plateaus correspond to time intervals in the low (high) field metastable operating point. If the actual photon number distribution is averaged over a time interval containing many spontaneous field jumps, the steady-state result $P(n)$ of the micromaser theory is recovered.

In the parameter ranges where switching occurs much faster than in the case shown in figure 3, the individual jumps cannot be resolved, therefore different methods have to be used for the measurement. Furthermore, hysteresis is observed at the maser parameters for which the field jumps occur. Owing to lack of space, these results cannot be discussed here. For a complete survey on the performed experiments it is referred to Benson *et al.* (1994).

In the following we would like to discuss the recent experiment on atomic interferometry in the micromaser (Raithel *et al.* 1995). Since a non-classical field is generated in the maser cavity, we were able for the first time to investigate atomic interference phenomena under the influence of non-classical radiation; owing to the
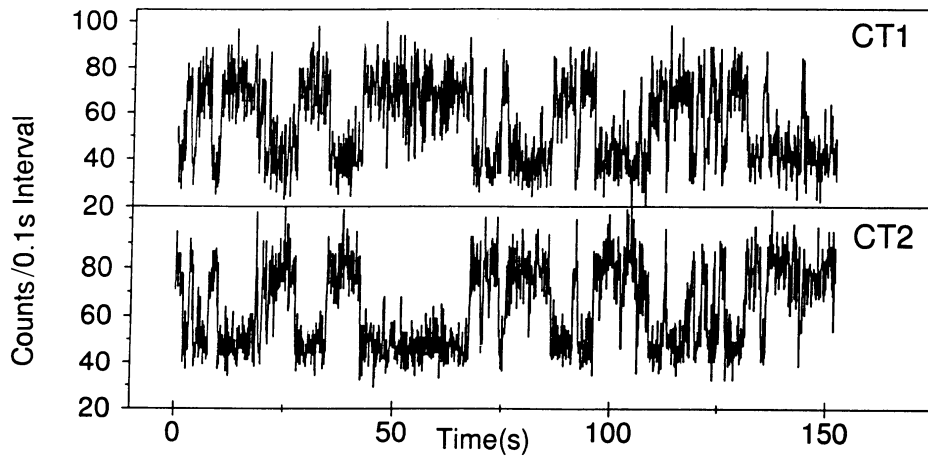
Figure 3. Quantum jumps between two equally stable operation points of the maser field. The channeltron counts are plotted versus time (CT1 = upper state and CT2 = lower state signals).

bistable behaviour of the maser field the interferences display quantum jumps, thus the quantum nature of the field gets directly visible in the interference fringes. Interferences occur since a coherent superposition of dressed states is produced by mixing the states at the entrance and exit holes of the cavity. Inside the cavity the dressed states develop differently in time, giving rise to Ramsey-type interferences (Ramsey 1956) when the maser cavity is tuned through resonance.

The set-up used in the experiment is identical to the one described before (Benson *et al.* 1994). However, the flux of atoms through the cavity is by a factor of 5–10 higher than in the previous experiments, where the $63P_{3/2}$–$61D_{5/2}$ transition was used. For the experiments, the Q value of the cavity was 6×10^9, corresponding to a photon decay time of 42 ms.

Figure 4 shows the standard maser resonance in the uppermost plot which is obtained when the resonator frequency is tuned. At large values of N_{ex} ($N_{ex} > 89$), sharp, periodic structures appear. These typically consist of a smooth wing on the low-frequency side, and a vertical step on the high-frequency side. The clarity of the pattern rapidly decreases when N_{ex} increases to 190 or beyond. We will see later that these structures have to be interpreted as interferences. It can be seen that the atom–field resonance frequency is red-shifted with increasing N_{ex}, the shift reaching 200 kHz for $N_{ex} = 190$. Under these conditions, there are roughly 100 photons on the average in the cavity. The large red-shift cannot be explained by AC Stark effect, which for 100 photons would amount to about one kHz for the transition used. Therefore, it is obvious that other reasons must be responsible for the observed shift.

It is known from previous maser experiments that there are small static electric fields in the entrance and exit holes of the cavity. It is supposed that this field is generated by patch effects at the surface of the niobium metal caused by rubidium deposits caused by the atomic beam or by microcrystallites formed when the cavities are tempered after machining. The tempering process is necessary to achieve high quality factors. The influence of those stray fields is only observable in the cavity holes; in the centre of the cavity they are negligible owing to the large atom–wall distances.

When the interaction time t_{int} between the atoms and the cavity field is increased, the interference structure disappears for $t_{int} > 47\,\mu s$ (Raithel *et al.* 1995). This is
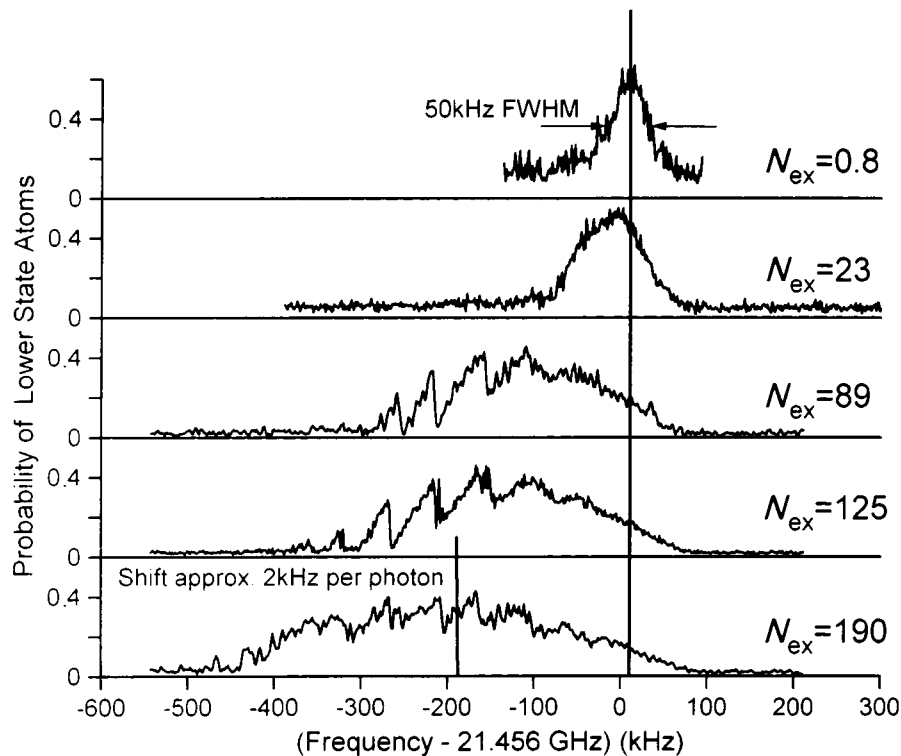
Figure 4. Shift of the maser resonance $63P_{3/2}$–$61D_{5/2}$ for fast atoms ($t_{int} = 35\,\mu s$). The upper plot shows the maser line for low pump rate ($N_{ex} < 1$). The FWHM linewidth (50 kHz) sets an upper limit of *ca.* 5 mV cm^{-1} for the residual electric stray fields in the centre of the cavity. The lower resonance lines are taken for the indicated large values of N_{ex}. The plots show that the centre of the maser line shifts by about 2 kHz per photon. In addition, there is considerable field-induced line broadening which is approximately proportional to $\sqrt{N_{ex}}$. For $N_{ex} \geqslant 89$, the lines display periodic structures, which are discussed in the text.

due to the fact that there is no non-adiabatic mixing any more between the substates when the atoms get too slow.

In order to understand the observed structures, we first have to analyse the Jaynes–Cummings dynamics of the atoms in the cavity. This treatment is more involved than that in connection with previous experiments, since the higher maser field requires detailed consideration of the field in the periphery of the cavity, where the additional influence of stray electric fields is more important.

The usual formalism for the description of the coupling of an atom to the radiation field is the dressed atom approach (Cohen-Tannoudji *et al.* 1992), leading to splitting of the coupled atom–field states, depending on the vacuum Rabi-flopping frequency Ω, the photon number n, and the atom–field detuning δ. We face a special situation at the entrance and exit holes of the cavity. There we have a position-dependent variation of the cavity field, as a consequence of which Ω is position dependent. An additional variation results from the stray electric fields in the entrance and exit holes. Owing to the Stark-effect, these fields lead to a position-dependent atom–field detuning δ.

The Jaynes–Cummings–Hamiltonian only couples pairs of dressed states. Therefore, it is sufficient to consider the dynamics within such a pair. In our case, prior

to the atom–field interaction, the system is in one of the two dressed states. For parameters corresponding to the periodic substructures in figure 4 the dressed states are mixed only at the beginning of the atom–field interaction and at the end. The mixing at the beginning creates a coherent superposition of the dressed states. Afterwards, the system develops adiabatically, whereby the two dressed states accumulate a differential dynamic phase Φ which strongly depends on the cavity frequency. The mixing of the dressed states at the entrance and exit holes of the cavity, in combination with the intermediate adiabatic evolution, generates a situation similar to a Ramsey two-field interaction.

The maximum differential dynamic phase Φ solely resulting from dressed-state coupling by the maser field is roughly 4Φ under the experimental conditions used here. This is not sufficient to explain the interference pattern of figure 4, where we have at least six maxima corresponding to a differential phase of 12π. This means that an additional energy shift differently affecting upper and lower maser states is present. Such a phenomenon can be caused by the above-mentioned small static electric fields present in the holes of the cavity. The static field causes a position-dependent detuning δ of the atomic transition from the cavity resonance; as a consequence we get an additional differential dynamic phase Φ. In order to interpret the periodic substructures as a result of the variation of Φ with the cavity frequency, the phase Φ has to be calculated from the atomic dynamics in the maser field.

The quantitative calculation can be performed on the basis of the micromaser theory. The calculations reproduce the experimental finding that the maser line shifts to lower frequencies when N_{ex} is increased (Raithel *et al.* 1995). The mechanism for that can be explained as follows. The high-frequency edge of the maser line does not shift with N_{ex} at all, since this part of the resonance is produced in the central region of the cavity, where practically no static electric fields are present. The low-frequency cut-off of the structure is determined by the location where the mixing of the dressed states occurs. With decreasing cavity frequency, those points shift closer to the entrance and exit holes, with the difference between the particular cavity frequency and the unperturbed atomic resonance frequency giving a measure of the static electric field at the mixing locations. Closer to the holes, the passage behaviour of the atoms through the mixing locations gets non-adiabatic for the following reasons. Firstly, the maser field strength reduces towards the holes. This leads to reduced repulsion of the dressed states. Secondly, the stray electric field strongly increases towards the holes. This implies a larger differential slope of the dressed state energies at the mixing locations, and therefore leads to a stronger non-adiabatic passage. At the same time, the observed signal extends further to the low frequency spectral region. Since the photon emission probabilities are decreasing towards lower frequencies, their behaviour finally defines the low-frequency boundary of the maser resonance line. With increasing N_{ex}, the photon number n increases. As for larger values of n, the photon emission probabilities get larger, also an increasing N_{ex} leads to an extension of the range of the signal to lower frequencies. This theoretical expectation is in agreement with the experimental observation.

In the experiment it is also found that the maser line shifts towards lower frequencies with increasing t_{int}. This result also follows from the developed model: the red-shift increases with t_{int} since a longer interaction time leads to a more adiabatic behaviour in the same way as a larger N_{ex} does.

The calculations reveal that on the vertical steps displayed in the signal the photon number distribution has two distinctly separate maxima similar to those observed at

the phase transition points discussed above. Therefore, the maser field should exhibit hysteresis and metastability under the present conditions as well. The hysteresis indeed shows up when the cavity frequency is linearly scanned up and down with a modest scan rate (Raithel *et al.* 1994). When the maser is operated in steady-state and the cavity frequency is fixed to the steep side of one of the fringes, we also observe spontaneous jumps of the maser field between two metastable field states.

The calculations also show that on the smooth wings of the more pronounced interference fringes the photon number distribution $P(n)$ of the maser field is strongly sub-Poissonian. This leads us to the conclusion that we observe Ramsey-type interferences induced by a non-classical radiation field. The sub-Poissonian character of $P(n)$ results from the fact that on the smooth wings of the fringes the photon gain reduces when the photon number is increased. This feedback mechanism stabilizes the photon number resulting in a sub-Poissonian photon distribution.

3. Entanglement in the micromaser

Owing to the interaction of the Rydberg atom with the maser field, there is an entanglement between field and state in which a particular atom is leaving the cavity. This entanglement was studied in several papers (see, for example, Wagner *et al.* 1993; Löffler *et al.* 1996). Furthermore, there is a correlation between the states of the atoms leaving the cavity subsequently. If, for example, atoms in the lower maser level are studied (see Walther 1992), an anticorrelation is observed in a region for the pump parameter Θ, where sub-Poissonian photon statistics is present in the maser field. Recently, measurements of these pair correlations have been performed giving a rather good agreement with the theoretical predictions by Briegel *et al.* (1994).

4. Conclusion

The presented maser model explains all the observed experimental facts. The periodic structures in the maser lines are thus interpreted as Ramsey-type interferences. If there was more accurate information on the DC fields in the cavity, a multilevel calculation taking into account the magnetic substructure of the involved fine-structure levels would make sense. Under the present conditions, however, the stray electric field amplitudes close to the cavity holes can only be estimated. The interference structure extends towards lower frequency as far as *ca.* 500 kHz for $N_{\mathrm{ex}} \approx 200$, this corresponding to an electric field of *ca.* 25 mV cm^{-1} in a distance of roughly a few mm from the cavity holes.

To our knowledge, it is the first time that it is demonstrated that non-adiabatic mixing can lead to Ramsey interferences. Besides other phenomena, the bistable character of the micromaser field can be observed in jumps of the fringes; the observed interferences thus show a discontinuous behaviour owing to the quantum properties of the field—it is the first time that such a discrete quantum behaviour is directly observed in interference fringes. One of the applications of the described Ramsey interferometer could be the quantum non-demolition measurement of the photon number in a cavity along the lines proposed by Brune *et al.* (1990). For this purpose, the atoms in the cavity have to be dispersively coupled to a third level via a second quantum field which could agree with the frequency of another cavity mode.

The observed entanglement between maser field and atoms and the pair correlations for atoms leaving the cavity is another proof for the richness of the micromaser.

References

Benson, O., Raithel, G. & Walther, H. 1994 Quantum jumps of the micromaser field—dynamic behavior close to phase transition points. *Phys. Rev. Lett.* **72**, 3506–3509.

Briegel, H.-J., Englert, B.-G., Sterpi, N. & Walther, H. 1994 One-atom maser: statistics of detector clicks. *Phys. Rev.* A **49**, 2962–2985.

Brune, M., Haroche, S., Lefevre, V., Raimond, J. M. & Zagury, N. 1990 Quantum non-demolition measurement of small photon numbers by Rydberg-atom phase-sensitive detection. *Phys. Rev. Lett.* **65**, 976–979.

Cohen-Tannoudji, C., Dupont-Roc, J. & Grynberg, G. 1992 In *Atom–photon interactions*, pp. 407–514. New York: Wiley.

Filipowicz, P., Javanainen, J. & Meystre, P. 1986 Theory of a microscopic maser. *Phys. Rev.* A **34**, 3077–3087.

Löffler, M., Englert, B.-G. & Walther, H. 1996 Testing a Bell-type inequality with a micromaser. *Appl. Phys.* B **63**, 511–516.

Lugiato, L. A., Scully, M. O. & Walther, H. 1987 Connection between microscopic and macroscopic maser theory. *Phys. Rev.* A **36**, 740–743.

Meschede, D., Walther, H. & Müller, G. 1985 The one-atom maser. *Phys. Rev. Lett.* **54**, 551–554.

Meystre, P. 1992 Cavity quantum optics and the quantum measurement process. In *Progress in optics* (ed. E. Wolf), vol. 30, pp. 261–355. New York: Elsevier.

Raimond, J. M., Brune, M., Davidovich, L., Goy, P. & Haroche, S. 1989 The two-photon Rydberg atom micromaser. *Atom. Phys.* **11**, 441.

Raithel, G., Wagner, C., Walther, H., Narducci, L. M. & Scully, M. O. 1994 The micromaser: a proving ground for quantum physics. In *Advances in atomic, molecular and optical physics* (ed. P. Berman), suppl. 2, pp. 57–121. New York: Academic.

Raithel, G., Benson, O. & Walther, H. 1995 Atomic interferometry with the micromaser. *Phys. Rev. Lett.* **75**, 3446–3449.

Ramsey, N. F. 1956 In *Molecular beams*, pp. 124–134. Oxford: Clarendon.

Rempe, G., Walther, H. & Klein, N. 1987 Observation of quantum collapse and revival in the one-atom maser. *Phys. Rev. Lett.* **58**, 353–356.

Rempe, G., Schmidt-Kaler, F. & Walther, H. 1990 Observation of sub-Poissonian photon statistics in a micromaser. *Phys. Rev. Lett.* **64**, 2783–2786.

Rempe, G. & Walther, H. 1990 Sub-Poissonian atomic statistics in a micromaser. *Phys. Rev.* A **42**, 1650–1655.

Wagner, C., Brecha, R. J., Schenzle, A. & Walther, H. 1993 Phase diffusion, entangled states and quantum measurements in the micromaser. *Phys. Rev.* A **47**, 5068–5079.

Wagner, C., Schenzle, A. & Walther, H. 1994 Atomic waiting-times and correlation functions. *Optics Comm.* **107**, 318–326.

Walther, H. 1992 Experiments on cavity quantum electrodynamics. In *Phys. Reports* **219**, 263–281.